Coherent ultrafast torsional motion and isomerization of a biomimetic dipolar photoswitch†

Julien Briand,[a] Olivier Bräm,[b] Julien Réhault,[c] Jérémie Léonard,[a] Andrea Cannizzo,[b] Majed Chergui,[b] Vinizio Zanirato,[d] Massimo Olivucci,[ef] Jan Helbing[c] and Stefan Haacke*[a]

Received 8th September 2009, Accepted 7th January 2010
First published as an Advance Article on the web 10th February 2010
DOI: 10.1039/b918603d

Femtosecond fluorescence up-conversion, UV-Vis and IR transient absorption spectroscopy are used to study the photo-isomerization dynamics of a new type of zwitterionic photoswitch based on a *N*-alkylated indanylidene pyrroline Schiff base framework (ZW-NAIP). The system is biomimetic, as it mimics the photophysics of retinal, in coupling excited state charge translocation and isomerization. While the fluorescence lifetime is 140 fs, excited state absorption persists over 230 fs in the form of a vibrational wavepacket according to twisting of the isomerizing double bond. After a short "dark" time window in the UV-visible spectra, which we associate with the passage through a conical intersection (CI), the wavepacket appears on the ground state potential energy surface, as evidenced by the transient mid-IR data. This allows for a precise timing of the photoreaction all the way from the initial Franck–Condon region, through the CI and into both ground state isomers, until incoherent vibrational relaxation dominates the dynamics. The photo-reaction dynamics remarkably follow those observed for retinal in rhodopsin, with the additional benefit that in ZW-NAIP the conformational change reverses the zwitterion dipole moment direction. Last, the pronounced low-frequency coherences make these molecules ideal systems for investigating wavepacket dynamics in the vicinity of a CI and for coherent control experiments.

Introduction

Photoisomerization is an elementary chemical reaction of fundamental importance in natural biological photoreceptors in which a protein cofactor seems to optimize the very reaction pathway of biological relevance (*e.g.* bR and Rho,[1–5] GFP,[6–8] or PYP[9–12]). Photoisomerization is the mechanism of choice to trigger large amplitude motion in molecular photo-switches such as those based on azobenzene (AB)[13,14] and used to photo-induce peptide folding,[15–17] control ion complexation[18] or gate the transport properties of ion channels by light.[19] The ideal molecular photo-switch would be characterized by a large photo-isomerization yield, a large photochromic contrast (absorption difference of E and Z forms), and the ability for optical resetting (E → Z → E).

Photoisomerization is currently described as a process involving a conical intersection (CI) between two electronic potential energy surfaces.[20] The theoretical and experimental investigation of the role of these CI's in a photo-chemical reaction is a subject of large interest.[21,22] In particular, the accurate prediction of the quantum yield of photoisomerization occurring through a CI remains out of reach since it depends critically on the environment of the chromophore which influences the structure of the CI itself, and involves crucial dynamic effects.[23,24]

The protonated retinal Schiff base (PSBR) chromophore of rhodopsin is an excellent model system to investigate photoisomerization. It is a Z/E photo-switch, bearing a record isomerization speed of 200 fs and quantum yield of more than 60%.[2,25] Quantitative computations of the excited state of PSBR in rhodopsin[21] have triggered the design of a new family of photoswitches, the *N*-alkylated indanylidene pyrroline Schiff bases (NAIP),[26] which mimic the photo-induced charge translocation and structural dynamics of the natural pigment. The biomimetic photoswitches have a single isomerizing bond, present one low-lying excited state, dissolve well in water and in other polar solvents and are small enough to be entirely manageable by state-of-the-art quantum chemistry methods.

[a] *Institut de Physique et Chimie des Matériaux de Strasbourg, UMR 7504, Strasbourg University, CNRS, IPCMS-DON, 23, rue du Loess, 67034 Strasbourg, France. E-mail: stefan.haacke@ipcms.u-strasbg.fr; Fax: (+33) 3 88 10 70 45; Tel: (+33) 3 88 10 7171*
[b] *Laboratoire de Spectroscopie Ultrarapide, ISIC – EPFL, BSP, CH-1015 Lausanne (CH)*
[c] *Physikalisch-Chemisches Institut, Universität Zürich, Winterthurerstrasse 190, 8057 Zürich, Switzerland*
[d] *Dipartimento di Scienze Farmaceutiche, Università di Ferrara, 44100 Ferrara, Italy*
[e] *Dipartimento di Chimica, Università degli Studi di Siena, 53100 Siena, Italy*
[f] *Chemistry Department, Bowling Green State University, Bowling Green, OH 43403, USA*

† Electronic supplementary information (ESI) available: Experimental equipment and conditions; ZW-NAIP preparation and UV-VIS steady-state characterization; femtosecond mid-IR experiments; transient UV-VIS absorption data processing; fluorescence and transient absorption data analysis; dynamics of the MeO-NABFP molecule. See DOI: 10.1039/b918603d

A methoxylated form of NAIP (MeO-NAIP) has been studied by quantum mechanics/molecular mechanics (QM/MM) computations, wavepacket dynamics simulations, and ultrafast spectroscopy, showing that in methanol (MeOH), MeO-NAIP displays excited state properties similar to those of the 11-*cis* PSBR embedded in rhodopsin.[26,27] In particular, upon light excitation a barrierless excited state profile drives the molecular system through a CI to the isomer within 0.3 ps. The 22% quantum yield is lower than in retinal proteins, clearly illustrating that high isomerization speed is not a sufficient condition for good reaction yield.

Here, we apply ultrafast fluorescence up-conversion and transient absorption techniques to study the excited and ground state dynamics of a chiral variant of the MeO-NAIP, named ZW-NAIP, in methanol. It is zwitterionic on the pyrroline moiety, so that isomerization entails a significant dipole moment inversion.[28] The present paper however, focuses on remarkable spectroscopic features, which suggest coherent motion to take place along the isomerization reaction coordinate. In the electronic spectra we observe a low-frequency vibrational wavepacket, which allows us to trace the dynamics of a coherent population all the way from the Franck–Condon region to the ground state photoproduct. The low-frequency excited-state wavepacket survives in the photoproduct's electronic ground state after passage through the CI, and a precise timing for the residence in this spectroscopically dark window is given. This opens up unique perspectives for detailed theoretical and experimental investigations of the wavepacket dynamics in the vicinity of a CI, and how the latter can be modified by external parameters.

The femtosecond UV-visible results on ZW-NAIP are complemented by the ones obtained by probing the mid-infrared (mid-IR) region. Vibrational spectroscopy better discriminates the two isomers and provides a continuous probe of the passage from the electronically exited state to the hot ground state and the subsequent cooling of the molecule.

Experimental methods

The UV-VIS fluorescence up-conversion and transient absorption set-ups are home-built, especially designed for broad spectral coverage in the 300–700 nm range. They offer a time resolution of 120 and 80 fs, respectively. In both experiments, the pump beam wavelength is 400 nm, and its intensity is kept in the linear regime of excitation, so as to promote the ZW-NAIP molecule to its first excited electronic state S_1 (see Fig. 1). All UV-VIS data presented in this paper are processed in order to compensate for group velocity dispersion and define accurately time zero at all wavelengths. In the case of transient absorption, the solvent and quartz capillary ultrafast cross-phase modulation signal is carefully measured and subtracted from the data.

Femtosecond mid-IR probe pulses (bandwidth 150 cm^{-1} FWHM) were generated by difference frequency generation of the Idler and Signal output of a home-built OPA, and detected together with a reference beam by a 32 pixels double array HgCdTe detector with 4 cm^{-1} resolution. Transient spectra were measured between 1475–1675 cm^{-1}. The time-resolution

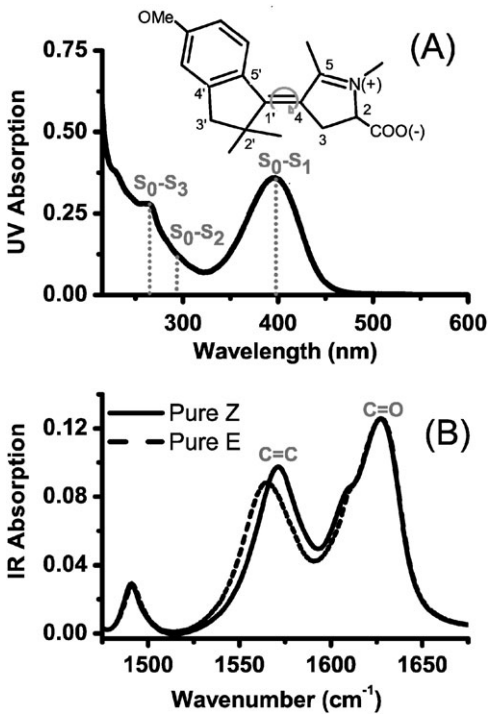

Fig. 1 (A) Electronic absorption spectrum of the ZW-NAIP (*Z*-isomer) photoswitch. The transitions are labelled according to ref. 28. Inset: The ZW-NAIP (Z)-isomer structure with an arrow around the isomerizing carbonyl bond. (B) FTIR spectra of the *Z*- and *E*-isomers (see text for band assignments). Optical densities are those used in the transient experiments, an 0.5 mm quartz cell for UV-Vis, and a 100 μm CaF_2 cell for IR measurements. The optical density at 390 nm corresponding to the IR spectrum is approximately 1.8.

of the set-up is 150 fs, as determined by measuring the pump-induced change in mid-IR-transmission of a germanium plate. Sample purity and isomer concentrations were checked shortly before and after measurements by recording ^{1}H-NMR spectra on a 300 MHz spectrometer (Bruker). No signs of molecular aggregation were found. In particular, the FTIR spectrum is concentration-independent far beyond the highest concentrations (20 mM) used in the transient IR experiments.

See the ESI† for further details about experimental conditions, data corrections and analysis.

Fig. 1A shows the structure and the electronic absorption spectrum of ZW-NAIP (Z), wherein the negative counterion is carried by a deprotonated carboxylate group (COO–) covalently bound to the pyrroline moiety. A racemic mixture has been synthesized according to procedures described in details elsewhere.[27–29] The UV-Vis absorption spectrum of the E form is blue-shifted by 6 nm and slightly more intense than the one of the Z isomer.[28] NMR spectroscopy indicates that more than 98% of the dark-adapted molecules are in the *Z*-isomer form.

The FTIR spectrum of ZW-NAIP in methanol (Fig. 1B) shows four bands in the spectral window between 1475 cm^{-1} and 1675 cm^{-1}, which can be compared with harmonic normal mode calculations (Gaussian program suite,[30] B3LYP with 6-31G+ basis set, see ESI.† The small band near 1490 cm^{-1} is due to CH_3 bending modes. The band at 1570 cm^{-1}, which

shifts most strongly upon isomerization, is assigned to a stretching mode dominated by in-phase contraction of the isomerizing C1′–C4 double bond and the C5–N bond of the pyroline moiety. The corresponding transition dipole moment is expected to be nearly parallel to the C1′–C4 bond and the electronic transition dipole moment, consistent with an anisotropy in the pump–probe data close to 0.4. Two normal modes involve strong asymmetric C=O stretching motion of the negatively charged carboxylate group (as well as out of phase C1′–C4 and C5–N stretch). One of them can be assigned to the 1626 cm^{-1} band, based on its slightly negative anisotropy in the pump–probe data and a predicted transition dipole moment nearly perpendicular to the C1′–C4 bond. The 1608 cm^{-1} shoulder may be attributed to the second mode involving C=O stretching or to a deformation of the 6-membered ring (equally involving some out of phase C1′–C4 and C5–N stretch motion).

Results and analysis

Mid-IR time-resolved absorption

Immediately after 390 nm excitation of a sample containing only *Z*-isomers, the mid-IR transient absorption spectrum in Fig. 2A (0.25 ps delay) is dominated by the bleaching of the 1570 cm^{-1} and 1630 cm^{-1} ground state absorption bands of ZW-NAIP. Comparison with the inverted FTIR spectrum (dashed line) reveals that between 1590 and 1620 cm^{-1} bleaching is weaker or partially compensated by induced absorption. (An additional, unstructured and fast-decaying offset due to the Kerr signal of the cell windows has been subtracted, see ESI.†) Between delays of 0.2 and 1 ps, an induced absorption signal is growing at the low frequency side of the C=C stretch band. Between 1 and 10 ps, its maximum is continuously shifting to higher wavenumbers, increasing the overlap of this induced band with the initial bleach (Fig. 1B). The 30 ps transient spectrum already resembles very closely the steady-state E–Z difference spectrum (Fig. 1C).

The measured transient IR spectra in Fig. 2A and B are difference spectra, composed of the absorption of the molecules after excitation minus their absorption before excitation. The latter contribution can be eliminated by subtracting a properly scaled FTIR spectrum (dashed line in Fig. 2A). This yields the "true" absorption spectra of photo-excited ZW-NAIP molecules from the moment of excitation up to the completion of the photoreaction; these spectra are shown in Fig. 2D and E. Growth and shifts of the vibrational bands can now be directly observed.

The band associated with the C=C stretch vibration disappears upon photoexcitation and grows in with a time constant of approximately 0.2 ps. This is indicated by the monoexponential fit to the integral signal shown by dotted symbols in Fig. 2 F, which is obtained by integration over the transient spectra between 1505 and 1590 cm^{-1} (vertical lines in Fig. 2A and B).

The complete disappearance of the 1570 cm^{-1} band upon photoexcitation is consistent with *ab initio* minimum energy path calculations, which predict loss of C=C double bond character in the S_1 excited state to occur prior to torsional

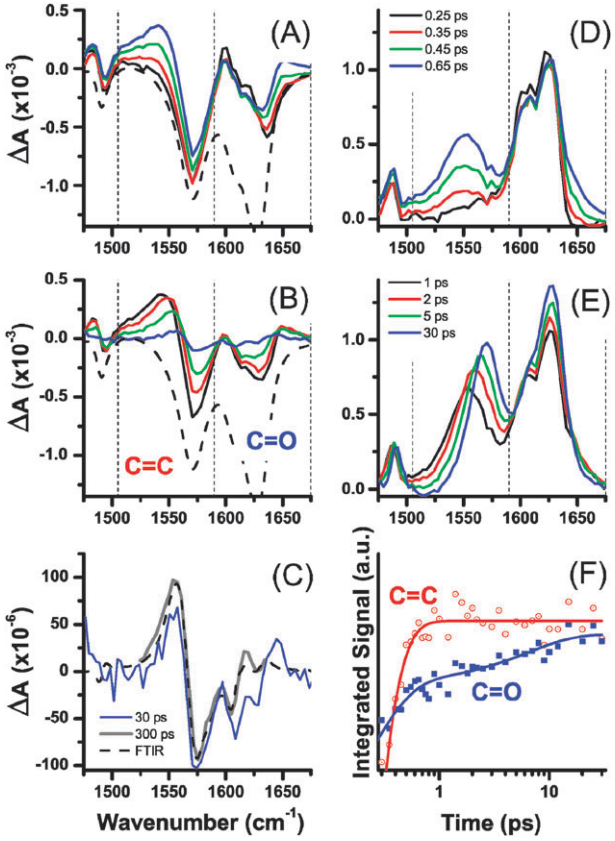

Fig. 2 (A) and (B) Transient absorption spectra at different delays after excitation at 390 nm of a sample containing only Z isomers. The dashed line is the scaled and inverted FTIR absorption spectrum. (C) Transient absorption after 30 ps (yellow), 300 ps (grey, highly averaged) and FTIR difference spectrum (dashed line). (D) and (E) Same data as in (A) and (B) after subtraction of the inverted absorption spectrum, which eliminates the bleaching component. (F) Integral of the transient spectra in A and B between vertical dashed lines at 1505 and 1590 cm^{-1} (C=C stretch, red open circles) and between 1590 and 1675 cm^{-1} (C=O stretch, solid squares). Solid lines in F represent mono-exponential (0.2 ps) and bi-exponential (0.2 and 5.5 ps) fits, respectively.

motion about the thus weakened C1′–C4 bond.[27,28] Its sub-picosecond reappearance is thus interpreted as a signature for the return of photo-excited molecules into the electronic ground state, as previously observed for MeO-NAIP.[26,27] At delays longer than 2 ps the essentially constant integrated signal in Fig. 2F indicates that electronic relaxation is complete, in agreement with the results of electronic spectroscopy presented below. On the picosecond timescale, the C=C stretch band is merely shifting and narrowing, as the initially hot molecules dissipate excess energy to the solvent.[31]

The C=O stretch band at 1630 cm^{-1} does not disappear, but only weakens and undergoes a red-shift immediately after photo-excitation. This leads to induced absorption that partially compensates the bleaching of the equally red-shifted 1608 cm^{-1} transition in Fig. 2A. Fast spectral changes on a sub-picosecond timescale comprise a decay of this red shift and a slight broadening of the C=O stretch band, which give rise to the positive absorption signal near 1650 cm^{-1} in the transient data of Fig. 2A. Unlike the C=C stretch mode

(1570 cm^{-1}), whose integrated intensity remains constant after 2 ps, the integral over the 1630 cm^{-1} band continues to grow on a picosecond timescale (solid squares in Fig. 2F). The charged carboxylate group thus shows an enhanced sensitivity to the solvation of the large permanent dipole due to rearrangement of the solvent structure.

From the fitting of the FTIR absorption spectrum to the 1570 cm^{-1} bleach signal in the early delay pump–probe spectra (0.25 ps signal in Fig. 2A), we can deduce the fraction of initially excited molecules. Matching the calibrated FTIR-difference and transient signal at 300 ps delay (Fig. 2C) then allows us to determine the final isomer ratio. This yields a 35% quantum efficiency for Z → E isomerization, that has to be seen as an upper limit, as the C=C stretch bleaching may be slightly underestimated due to spectral overlap.

UV/VIS time-resolved emission and absorption

A time-resolved fluorescence 2D map of the ZW-NAIP in methanol is presented in Fig. 3A. The emission spectrum extends from 440 to 670 nm, with a maximum close to 520 nm, *i.e.* more than 120 nm (6020 cm^{-1}) red-shifted from the absorption peak. A typical kinetic trace (at 502 nm) is shown in Fig. 3B together with a fit to a bi-exponential decay curve. The signal rises within the instrument response function (IRF) and decays with two time constants $\tau_1 = 0.14 \pm 0.01$ ps and $\tau_2 = 0.99 \pm 0.06$ ps. The same two time constants are enough to fit accurately the data at all wavelengths. Fig. 2C shows amplitude spectra associated with each time constant (decay associated spectra-DAS, see ESI for details†) resulting from a global fit analysis. The two DAS overlap with the same maximum (~520 nm) and spectral width of 110 nm (4200 cm^{-1}). This indicates that both components are related to populations residing in the same fluorescent window, with the large majority (~90%) leaving it within 0.14 ps.

Unlike the fluorescence and mid-IR data, the electronic transient absorption displays pronounced dynamic spectral shifts and coherent oscillations pointing to a wave-packet-like population in both excited and ground states. This is highlighted in Fig. 4A, which presents a 2D-map of the pump-induced absorbance changes (ΔA) in the range of 300–700 nm as a function of an up to 5 ps time-delay between pump and probe pulses. Negative ΔA, coded in blue, is due to ground state bleach (GSB) or stimulated emission (SE), while positive, red-coded ΔA represents excited-state absorption (ESA) or photoproduct absorption (PA) bands. Excited-state dynamics is observed during the first 0.3 ps, followed by internal conversion ($S_1 \rightarrow S_0$), oscillations (see pink areas around 450 nm in Fig. 4A, and Fig. 5 below) and thermalization in the ground state beyond 0.3 ps. Fig. 4B and C present selected spectra and kinetic traces from the same data set.

The time-zero transient spectrum (see Fig. 4B) shows two narrow positive and negative structures at 379 nm and 425 nm, respectively. They constitute an instantaneous stimulated Raman amplification (SRA) signal due to a ~1600 cm^{-1} ZW-NAIP vibrational mode, which is sufficiently coupled to the optical excitation to be clearly observed in our experiment (see also ESI).† Besides, stimulated emission (SE, $\Delta A < 0$) is observed from ~450 nm to the red-most part of the spectrum. At $t = 0.15$ ps, this SE signal is largest around 520 nm, in very good agreement with the above fluorescence data. The apparent spectral evolution of SE from 0 to 0.15 ps is due to the presence of a fast decaying excited-state absorption (ESA1), most clearly seen in the $t = 0$-ps spectrum (Fig. 4B) from 600 to 700 nm. This long-wavelength ESA1 rises and decays within the IRF and dominates the SE in the first

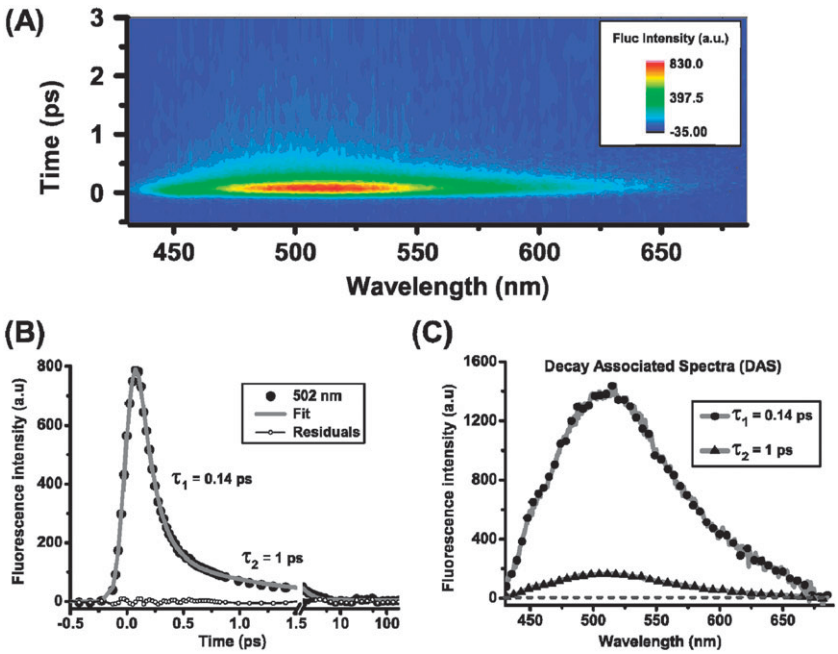

Fig. 3 (A) Time- and wavelength-resolved fluorescence up-conversion data. (B) Kinetic trace at 502 nm (black dots) together with a bi-exponential fit (gray line, decay constants: 0.14 ps and 0.99 ps) and the corresponding residuals. (C) Results of a global analysis of the whole fluorescence up-conversion data set. The amplitude ratio is 0.87/0.13, almost wavelength-independent.

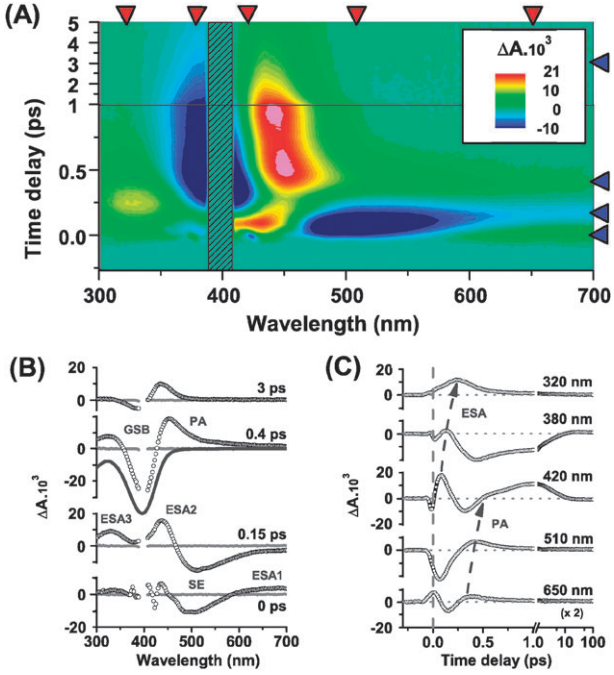

Fig. 4 (A) 2D map of the UV-Vis transient absorption change ΔA of ZW-NAIP in methanol as a function of wavelength and time delay. The time scale is enlarged between −0.25 and 1 ps. The color scale is chosen to highlight specific, lower-amplitude features discussed in the text, hence pink and dark blue represent larger amplitude, out-of-scale data. Because of enhanced noise due to pump scattering around 400 nm, the crossed-out portion is disregarded. (B) Time-resolved spectra (open circles) at delays indicated by the cursors on the right of panel A. The zero signal level is defined by negative-delay (−0.2 ps) spectra (gray lines). Along with the 0.4-ps spectrum, the inverted ground state absorbance is shown (solid line). (C) Selected kinetic traces at wavelengths indicated by the cursors on the top of panel A. Curved arrows highlight the spectral shift of excited-state absorption (ESA) and photoproduct absorption (PA).

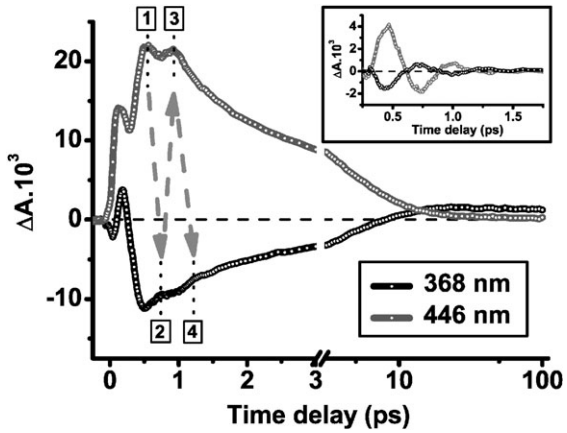

Fig. 5 (A) Selected kinetic traces on blue (black) and red (grey) sides of the $S_0 \rightarrow S_1$ ZW-NAIP absorption. Antiphased oscillations (numbered 1 to 4) are associated to coherent vibrational motion in the ground state. Dashed arrows are guides to the eye. The first positive peak, however, is due to ESA (see text). (B) Oscillatory part of the signals at 368 (black) and 446 nm (grey) obtained by subtracting the incoherent kinetics contributions from the raw data.

~100 fs (*cf.* kinetic trace at 650 nm, Fig. 4C). It is most probably a signature of molecules located in the Franck–Condon region.

At shorter wavelengths, two positive absorption bands labeled ESA2 and ESA3 are observed, which are best seen at 0.15 ps (see Fig. 4B) with their maxima at 420 and 320 nm, respectively. While ESA2 appears approximately within the IRF, ESA3 is clearly delayed in time (Fig. 4A and C), and reaches its maximum at $t = 0.23$ ps only, showing pronounced, non-exponential rise and decay kinetics. In addition, a close inspection of the transient signal at 380 nm (Fig. 4C) shows a small positive contribution peaking at ~120 fs, which is attributed to an ESA overcoming the GSB. Therefore we conclude that ESA2 and ESA3 are a single ESA band associated to the same $S_1 \rightarrow S_n$ transition, which spreads over the GSB contribution and spectrally shifts (see dashed arrow on Fig. 4C) from 450 nm at time zero, to 330 nm at $t = 0.23$ ps, as a result of the excited-state wavepacket dynamics.

Then, the 510 nm kinetic trace (Fig. 4C) clearly shows a break in its slope at $t \sim 0.2$ ps. It is caused by a delayed, rapidly decaying absorption signal (see ESI for detailed discussion),† which follows the initial SE signal and peaks at 380 fs. This is a time delay significantly larger than the average fluorescence lifetime and occurring about 150 fs after the maximum of ESA3. Hence we assign it to ground state photoproduct absorption (PA), also in analogy with the non zwitterionic variant.[27] PA designates hereafter pump-induced absorption features in the ground state, regardless of them being due to either the Z or E isomer. The time-delayed PA signal is very broad (450–720 nm, see the 0.4-ps spectrum Fig. 4B and the 650-nm transient Fig. 4C) and very rapidly narrows within ~50 fs, giving rise to the first peak (pink region around 0.5 ps in Fig. 4A) of a series of rapidly damped oscillations. The latter alternatively modulate two bands, which are a positive band between 420 and 470 nm attributed to the PA of an incoherent, vibrationally hot population, and a negative band between 350 and 420 nm associated to GSB (*cf.* comparison of the 0.4-ps spectrum and steady-state transmission in Fig. 4B). As shown in Fig. 5, the oscillations are best seen in the blue (368 nm) and red edges (446 nm) of the ground state absorption spectra of both isomers, corresponding to the wavepacket turning points. They can be isolated from the underlying incoherent kinetics (see inset and data analysis below), and appear antiphased, as expected for a wave packet oscillating around the ground-state equilibrium position. Subsequent swinging and damping give rise to a series of 2 to 3 oscillation maxima, persisting for almost 1.5 ps.

Damping of the ground state coherences goes along with thermalization processes, which shift the PA maximum towards 420 nm, and lead to partial GSB recovery in the 3-ps spectrum (Fig. 4B). Further evolution over ~30 ps leads to an almost pure E–Z difference spectrum (*cf.* "infinite" DADS Fig. 7), in agreement with the above femtosecond mid-IR data.

A quantitative analysis of the data is now presented. The kinetics observed appear to be a mixture of wave-packet-like motion showing dynamically shifting bands and oscillations,

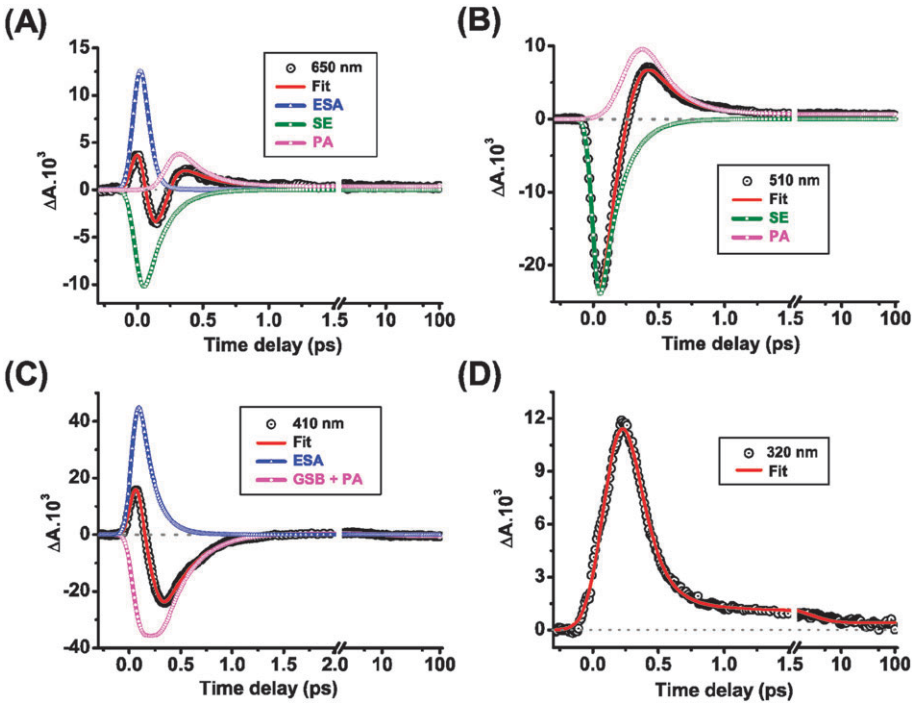

Fig. 6 Selected kinetic traces (black dots) and corresponding fits (red lines) at (A) 650 nm, (B) 510 nm, (C) 410 nm and (D) 320 nm. The different contributions to the fitting functions are identified as ESA (blue), SE (green) and ground state signals, GSB or PA (pink). See text for details.

and non-coherent relaxation. The quantitative timing associated to the spectrally shifting UV ESA and the delayed onset of the PA can be obtained by fitting a selection of representative kinetic traces. Fig. 6 displays the results of such fits and decomposition into the different overlapping transitions described above. The traces do not obey purely exponential kinetics like those derived from rate equation models (see the ESI for detailed discussion of the fitting procedure).† Rather, the fitting function of choice is the convolution of a Gaussian function, representing the IRF in most cases, to a sum of exponential decaying functions, possibly starting after a time-delayed onset, or modulated by a sine wave if needed. At 650 and 510 nm (Fig. 6A and B), the instantaneous contributions (IRF-limited rise time) are assigned to SE (green) and ESA1 (blue). The delayed contribution is due to PA (pink), according to the above discussion. At 410 nm, instantaneous contributions are associated with GSB (pink) and ESA2 (blue). Here the delayed component causes sudden recovery of the negative contribution after an unusual plateau. It is interpreted as the delayed PA onset together with partial bleach recovery. The GSB being initially constant is behaviour assumed *a priori*, consistent with the delayed PA onset at larger wavelengths. This assumption is justified by the good fit quality at 410 nm and by failure of alternative fit scenarios (see ESI).†

At 320 nm the steady-state absorption is minimum (Fig. 1A), and so is the GSB. Consequently, ESA3 is observed almost pure (Fig. 6D). The rise of the signal is significantly slower than the IRF and is fitted with a Gaussian function of 290 fs FWHM, time-shifted by 130 fs with respect to time zero. In line with the above discussion, this underscores ESA3 being the result of a gradual spectral shift of the ESA band, in contrast to the IRF-limited rise of ESA2 at 410 nm. The 200-fs time scale of the shift suggests that the excited state wavepacket progresses along a low-frequency, torsional mode. Then, the fitting of single transients from 650 to 410 nm (Fig. 6A–C) yields the time-shift of the delayed component, that is the onset time of the PA. It continuously evolves from 240 fs at 650 nm to 300 fs at 410 nm. This trend strongly supports the picture of a vibrational wavepacket arriving impulsively in the ground state, and evolving rapidly towards the potential energy minimum. Similar delayed fitting functions are also used to extract the non-coherent kinetics underlying the oscillatory part of the transients at 368 and 446 nm displayed in Fig. 5. Both oscillatory residuals are fitted with a common period and damping time (see ESI for details).† They yield a period of 560 fs ($\sim$60 cm^{-1}) and a decoherence time of $\sim$320 fs, characterizing the subsequent oscillatory behaviour of the vibrational wavepacket in the ground state.

The wavepacket arrival time is in good agreement with the C=C stretch band recovery found by mid-IR spectroscopy. Due to longer pulse durations, perturbed free induction decay (PFID) signals at negative pump–probe delay and a Kerr-signal from the sample cell windows, the mid-IR experiment cannot unambiguously distinguish between an instantaneous or a delayed onset of ground state population. Nevertheless, the 0.25 ps spectrum in Fig. 2D, which is the first one free of PFID and Kerr-signal contributions, shows only a very small positive C=C stretch band.

Finally, after 1.2 ps, oscillations and dynamical spectral shifts have vanished. Therefore, singular value decomposition (SVD) and global fitting with conventional sums of exponential functions are appropriate. Fig. 7 shows the decay associated difference spectra (DADS) of the three time

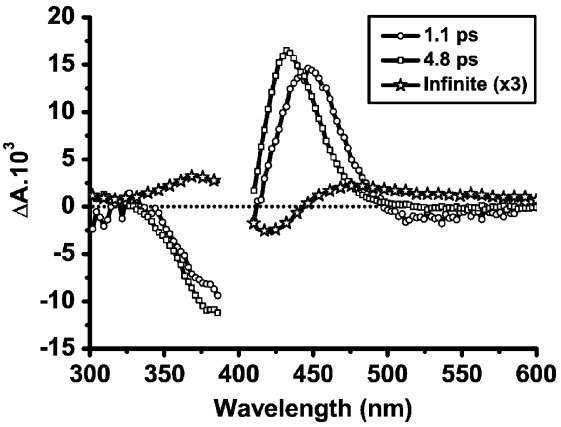

Fig. 7 Decay associated difference spectra (DADS) of the slowest components of the transient absorption data of ZW-NAIP. The two major decay components of 1.1 and 4.8 ps are related to solvation/IVR and cooling.

constants resulting from this analysis. The "infinite" time constant DADS shows the E–Z difference spectrum, and additional absorption for $\lambda > 450$ nm. The origin of this feature is unclear, but probably related to repetitive photo-excitation, since it is not observed with freshly prepared photoswitches.[32] In the range 400–500 nm the shorter-lived 1.1-ps DADS is ~20 nm red-shifted with respect to the longer-lived, 4.8-ps one, indicating ground-state solvation or intramolecular vibrational relaxation (IVR), and subsequent cooling, in agreement with MeO-NAIP[27] and the mid-IR data. Finally, the weak negative SE amplitude in the 1.1-ps DADS at $\lambda > 500$ nm is in line with the small 1-ps decay component found in the time-resolved fluorescence (see above).

Discussion

In photo-isomerizing systems, periodic oscillatory signals commonly assigned to vibrational coherences, have been observed in various molecular systems in solution, both in the excited state[33–37] as well as in the ground state.[38–40] In most cases, ground-state coherent vibrational dynamics result from resonant impulsive Raman scattering (RIRS), a process in which the pump beam impulsively populates Raman-active vibrational modes in the ground state, provided the pump pulse duration is appropriate.[41,42] For protein-bound retinal and similar isomerizing molecules, Raman active ground state vibrational modes in the range 1000–1500 cm^{-1} were observed.[36,38,39] However, in these systems, low-frequency RIRS in the range 60 cm^{-1} has not been reported, even in experiments performed with favourable pump pulse durations.[35] Only in the case of rhodopsin, a 60 cm^{-1} mode was observed *in the photoproduct all-trans state*, associated with torsion around retinal's isomerizing double bond.[40]

Similarly, here we argue that the observed 60-cm^{-1} oscillations are not produced by RIRS, but are the signature of a wave packet initially created in the excited state, which survives in the photoproduct after crossing the conical intersection. First, low-energy torsional modes are known to have negligible Raman activity as compared to high frequency modes.[43] Second, we can compare the present case of ZW-NAIP, to a similar molecule from the IP family, methoxy *N*-alkylated benzofuranylidene pyrroline (MeO-NABFP), which differs from the earlier reported MeO-NAIP[27] in that an oxygen atom substitutes a carbon in the indanylidene moiety (see ESI).† Besides a negligible effect on the ground state torsional frequency, the substitution should not affect the possibility of a low-frequency RIRS signal, and yet such a feature is absent in the MeO-NABFP data. Rather, due to the modified charge distributions, and potential energy surfaces, the MeO-NABFP photoswitch shows a 600 fs excited state lifetime, and exponential decay kinetics (see ESI).† We conclude that in BFP, as a consequence of the longer excited state lifetime, coherence is lost to a large extent already in the excited state. This conclusion is in line with the behaviour of metal carbonyls in the gas phase.[44]

The ZW-NAIP data reported above show that the molecules evolve in concert according to a coherent vibrational motion first on the excited state, then in the ground state while dispersing into an incoherent vibrationally unrelaxed population. Remarkably, this relatively well-focussed population can be tracked in time, leading to the following scenario. At $t = 0$, optical excitation is strongly coupled to a vibrational mode around 1600 cm^{-1}, as highlighted by the stimulated Raman signal in the $t = 0$ spectra (Fig. 4B), which most likely is a C=C stretch. This observation supports the existence of a π–π^* transition with bond order change, which weakens the isomerizing double bond,[26,27] as directly evidenced by the mid-IR bleach band. Fluorescence, stimulated emission as well as ESA 1 and 2 bands are then observed to occur within the IRF and to decay with times of ~0.15 ps (~90% amplitude) and ~1 ps (~10%). The latter is most probably associated with slower reacting Z isomers, and not with a small concentration of E, as the E → Z backward reaction is as fast as the forward reaction.[32,45] The faster majority population undergoes wavepacket-like motion on the excited state manifested by the ESA blue-shift with the blue-most ESA3 being maximal at 0.23 ps. Since the fluorescence has largely decayed at that moment, the time-delayed ESA3 band should be associated with excited-state molecules in a non-fluorescent geometry, that is in a geometry significantly different from the ground-state equilibrium one. As a matter of fact, we have previously shown for the sister compound MeO-NAIP that the S_1–S_0 transition dipole moment significantly drops as the isomerizing bond is twisted.[27] Unlike fluorescence, the ESA allows us to follow the wave packet along a low-frequency motion towards the region of configuration space where internal conversion to the ground state occurs. Then the broad VIS PA band emerges suddenly after a wavelength-dependent delay of 240 to 300 fs, and reaches its maximum at $t = 380$ fs, that is approximately 150 fs after the maximum of ESA3. In the present situation of coherent reaction dynamics, this means that during a ~150-fs time window the vibrational wavepacket created in S_1 produces no signature other than that that related to its temporal spreading (*cf.* width of the 320-nm transient, Fig. 4C). Therefore, we attribute this 150-fs time window to the passage through a "spectroscopically dark" volume of conformational space around a conical intersection. Consequently, this early PA signature should be

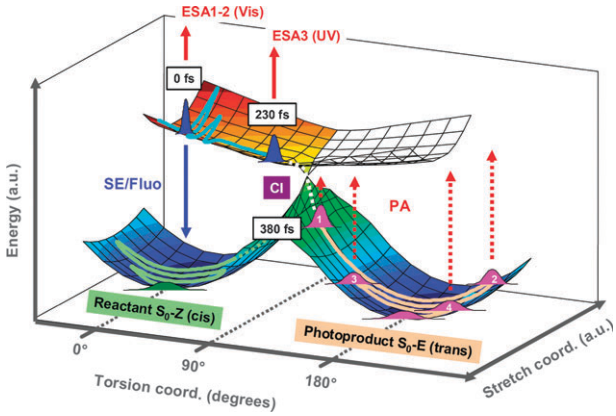

Fig. 8 Proposed scenario and timing for ZW-NAIP's photo-reaction. Immediately after photoexcitation, ESA and emission (SE/Fluo) are observed. While the molecules leave the fluorescent window, the ESA band spectrally shifts, reflecting motion along the torsional coordinate. After a spectroscopically dark period, associated with the passage through the conical intersection, the molecules populate the ground state in both isomer confirmations in form of an oscillating, rapidly damped wavepacket with $a \approx 560$ fs period, schematically indicated by turning points 1 to 4, along the reaction coordinate. As explained in the text, both ground state Z and E potentials are populated in parallel.

attributed to molecules arriving impulsively in the ground state *after* internal conversion. Once in the ground state, the wavepacket undergoes strongly damped vibrational oscillations, whose frequency of 60 cm^{-1} is consistent with torsional motion around the central C=C bond. Damping of these oscillations goes along with formation of an incoherent, vibrationally-excited population. Finally, the first spectroscopic evidence of the E isomer as a positive ΔA only emerges after vibrational relaxation has sufficiently progressed to narrow the Z bleach and E photoproduct bands, much like in the transient mid-IR spectra. After 30 ps, a quasi-static Z/E difference spectrum is reached. This scenario of wave-packet-like photo-isomerization is depicted in Fig. 8.

In the present case, due to the small differences of Z and E VIS absorption spectra, it is difficult to assign the ground-state torsional wavepacket and the "vibrationally hot" PA to one of the two isomers. Actually, in the light of the isomerization yield ($\leq$35%), these signals are most probably dominated by the majority of *Z*-like conformers. However, the branching into Z or E ground states occurs at the conical intersection, that is during the "dark time window". Therefore, both conformers are (re-)formed on the same time scale. The 0.38-ps occurrence time of maximum PA signal should thus be considered as the isomerization time, in line with mid-IR spectroscopy which clearly shows that reformation of the C=C double bond characteristic of the ground state happens within less than 0.3 ps.

Tied together, these observations give strong support to previous theoretical investigations of similar molecules, which do predict that optical excitation initially triggers C=C stretch relaxation which transfers part of its kinetic energy into a low-frequency, torsional mode.[27] This reactive mode drives the system towards the conical intersection back into the (photoproduct) ground state and the internal conversion is associated with isomerization. The 0.23-ps excited-state propagation time observed here for ZW-NAIP is in good agreement with the predicted 180-fs evolution along the torsional mode for MeO-NAIP.[27] Here we emphasize that in the present limit of coherent reaction dynamics, the ability to track the wavepacket dynamics clearly shows that the fluorescence lifetime is significantly shorter than the formation of the ground state photoproduct. This is in contrast to "slowly" isomerizing systems, for which fluorescence lifetimes and photoproduct formation times are equal.[1,4,5,46,47]

According to the above scenario, the coherent character of the photo-reaction bears a lot of similarity with that of retinal in rhodopsin.[2] Blue-shifting ESA has been observed on sub-50 fs time scales in retinal proteins,[48–50] most probably reflecting the initial high-frequency stretch relaxation of retinal. Isorhodopsin is similar to ZW-NAIP in that the excited-state wavepacket proceeds on time scales longer than the SE.[50] In both ZW-NAIP and rhodopsin cases, the SE is similarly short and followed by a rapid red (ZW-NAIP) or near-IR (rhodospin) induced absorption,[51] preceding the ground state wave packet dynamics.[40] By analogy with the very short-lived PA in ZW-NAIP, the rhodospin near-IR band should be attributed to the wavepacket arrival in the photoproduct state, as suggested in ref. 52. The simplified two-state/two-mode model initially proposed for the photo-reaction of retinal proteins[53] accounts well for the coherent and incoherent reaction dynamics of ZW-NAIP.

Conclusions

The goals of "biomimetic" design have been achieved in terms of reaction speed and torsional coherences. However, even though the excited and ground state dynamics appear to be remarkably similar, the photoproduct quantum yield of ZW-NAIP remains lower ($\leq$35%) than that of rhodopsin ($\sim$66%). This demonstrates that high speed and coherence of the excited state wavepacket are not sufficient for a high quantum yield.[40] Topological details of the CI, possibly modified by the environment, may influence it as well.[23,54]

To the best of our knowledge, apart from retinal in rhodospin, ZW-NAIP as well as MeO-NAIP are the only isomerizing molecules in solution in which vibrational coherence produced in the excited state is observed in the ground state after the passage through a conical intersection. One may conjecture this to be a common feature for molecules in which the excited state lifetime is on the order of or shorter than half the torsional period.[55] This requires not only a barrierless excited state but also high enough kinetic energy to be transferred from the optically excited high-frequency modes into the torsional motion around the isomerizing bond.

The NA-IP photoswitches offer the possibility (a) to track the wavepacket dynamics *via* UV-VIS transition absorption and pronounced non-exponential reaction dynamics and (b) to compute accurate potential energy surfaces and wavepacket dynamics.[27] Therefore it is an ideal system to investigate both experimentally and theoretically the properties of conical intersections, and the physical processes which govern the quantum yield. Experimental evidence of these wavepacket dynamics could also lead to a coherent control approach of

isomerization.[56–58] In addition, the C=O stretch band of the zwitterion's carboxylate group provides an unusual vibrational probe of the short-lived electronically excited state, which may be exploited further in structure-sensitive experiments.[59]

Finally, like MeO-NAIP, the zwitterion is a good candidate for a novel chiral molecular photoswitch, with an additional, remarkable property: here the isomerization leads to a difference in dipole moment as large as ~30 Debye.[28] This opens new potential applications for this nanoswitch, transducing light into both mechanical and electrostatic energy, and will be addressed in our future work.

References

1 J. Dobler, W. Zinth, W. Kaiser and D. Oesterhelt, *Chem. Phys. Lett.*, 1988, **144**, 215–220.
2 R. W. Schoenlein, L. A. Peteanu, R. A. Mathies and C. V. Shank, *Science*, 1991, **254**, 412–415.
3 H. Kandori, Y. Furutani, S. Nishimura, Y. Shichida, H. Chosrowjan, Y. Shibata and N. Mataga, *Chem. Phys. Lett.*, 2001, **334**, 271–276.
4 P. Hamm, M. Zurek, T. Röschinger, H. Patzelt, D. Oesterhelt and W. Zinth, *Chem. Phys. Lett.*, 1996, **263**, 613–621.
5 G. Zgrablić, S. Haacke and M. Chergui, *J. Phys. Chem. B*, 2009, **113**, 4348.
6 M. Chattoraj, B. A. King, G. U. Bublitz and S. G. Boxer, *Proc. Natl. Acad. Sci. U. S. A.*, 1996, **93**, 8362–8367.
7 H. Lossau, A. Kummer, R. Heinecke, F. Pöllinger-Dammer, C. Kompa, G. Bieser, T. Jonsson, C. M. Silva, M. M. Yang, D. C. Youvan and M. E. Michel-Beyerle, *Chem. Phys.*, 1996, **213**, 1.
8 N. M. Webber, K. L. Litvinenko and S. R. Meech, *J. Phys. Chem. B*, 2001, **105**, 8036–8039.
9 A. Baltuska, I. H. M. van Stokkum, A. Kroon, R. Monshouwer, K. J. Hellingwerf and R. van Grondelle, *Chem. Phys. Lett.*, 1997, **270**, 263.
10 H. Chosrowjan, N. Mataga, N. Nakashima, Y. Imamoto and F. Tokunaga, *Chem. Phys. Lett.*, 1997, **270**, 267.
11 P. Changenet-Barret, P. Plaza and M. M. Martin, *Chem. Phys. Lett.*, 2001, **336**, 439.
12 D. S. Larsen, M. Vengris, I. H. M. van Stokkum, M. A. van der Horst, F. L. de Weerd, K. J. Hellingwerf and R. van Grondelle, *Biophys. J.*, 2004, **86**, 2538.
13 I. K. Lednev, T. Q. Ye, P. Matousek, M. Towrie, P. Foggi, F. V. R. Neuwahl, S. Umapathy, R. E. Hester and J. N. Moore, *Chem. Phys. Lett.*, 1998, **290**, 68.
14 T. Nägele, R. Hoche, W. Zinth and J. Wachtveitl, *Chem. Phys. Lett.*, 1997, **272**, 489.
15 L. Ulysse, J. Cubillos and J. Chmielewski, *J. Am. Chem. Soc.*, 1995, **117**, 8466–8467.
16 S. Rudolph-Bohner, M. Krüger, D. Oesterhelt, L. Moroder, T. Nägele and J. Wachtveitl, *J. Photochem. Photobiol., A*, 1997, **105**, 235.
17 J. Bredenbeck, J. Helbing, A. Sieg, T. Schrader, W. Zinth, C. Renner, R. Behrendt, L. Moroder, J. Wachtveitl and P. Hamm, *Proc. Natl. Acad. Sci. U. S. A.*, 2003, **100**, 6452–6457.
18 S. Shinkai, T. Nakaji, Y. Nishida, T. Ogawa and O. Manabe, *J. Am. Chem. Soc.*, 1980, **102**, 5860–5865.
19 M. R. Banghart, M. Volgraf and D. Trauner, *Biochemistry*, 2006, **45**, 15129–15141.
20 B. G. Levine and T. J. Martinez, *Annu. Rev. Phys. Chem.*, 2007, **58**, 613–634.
21 P. B. Coto, A. Sinicropi, L. De Vico, N. Ferr and M. Olivucci, *Mol. Phys.*, 2006, **104**, 983.
22 A. Migani, A. Sinicropi, N. Ferré, A. Cembran, M. Garavelli and M. Olivucci, *Faraday Discuss.*, 2004, **127**, 179–191.
23 A. Toniolo, S. Olsen, L. Manohar and T. J. Martinez, *Faraday Discuss.*, 2004, **127**, 149–163.
24 I. Burghardt, L. S. Cederbaum and J. T. Hynes, *Comput. Phys. Commun.*, 2005, **169**, 95.
25 J. Tittor and D. Oesterhelt, *FEBS Lett.*, 1990, **263**, 269–273.
26 F. Lumento, V. Zanirato, S. Fusi, E. Busi, L. Latterini, F. Elisei, A. Sinicropi, T. Andruniów, N. Ferré, R. Basosi and M. Olivucci, *Angew. Chem., Int. Ed.*, 2007, **46**, 414–420.
27 A. Sinicropi, E. Martin, M. Ryazantsev, J. Helbing, J. Briand, D. Sharma, J. Léonard, S. Haacke, A. Cannizzo, M. Chergui, V. Zanirato, S. Fusi, F. Santoro, R. Basosi, N. Ferré and M. Olivucci, *Proc. Natl. Acad. Sci. U. S. A.*, 2008, **105**, 17642–17647.
28 A. Melloni, R. R. Paccani, D. Donati, V. Zanirato, A. Sinicropi, M. L. Parisi, E. Martin, R. Basosi, S. Fusi, L. Latterini, N. Ferré and M. Olivucci, submitted, 2009.
29 V. Zanirato, G. P. Pollini, C. De Risi, F. Valente, A. Melloni, S. Fusi, J. Barbetti and M. Olivucci, *Tetrahedron*, 2007, **63**, 4975.
30 M. J. Frisch, G. W. Trucks, H. B. Schlegel, G. E. Scuseria, M. A. Robb, J. R. Cheeseman, J. A. J. Montgomery, T. Vreven, K. N. Kudin, J. C. Burant, J. M. Millam, S. S. Iyengar, J. Tomasi, V. Barone, B. Mennucci, M. Cossi, G. Scalmani, N. Rega, G. A. Petersson, H. Nakatsuji, M. Hada, M. Ehara, K. Toyota, R. Fukuda, J. Hasegawa, M. Ishida, T. Nakajima, Y. Honda, O. Kitao, H. Nakai, M. Klene, X. Li, J. E. Knox, H. P. Hratchian, J. B. Cross, C. Adamo, J. Jaramillo, R. Gomperts, R. E. Stratmann, O. Yazyev, A. J. Austin, R. Cammi, C. Pomelli, J. W. Ochterski, P. Y. Ayala, K. Morokuma, G. A. Voth, P. Salvador, J. J. Dannenberg, V. G. Zakrzewski, S. Dapprich, A. D. Daniels, M. C. Strain, O. Farkas, D. K. Malick, A. D. Rabuck, K. Raghavachari, J. B. Foresman, J. V. Ortiz, Q. Cui, A. G. Baboul, S. Clifford, J. Cioslowski, B. B. Stefanov, G. Liu, A. Liashenko, P. Piskorz, I. Komaromi, R. L. Martin, D. J. Fox, T. Keith, M. A. Al-Laham, C. Y. Peng, A. Nanayakkara, M. Challacombe, P. M. W. Gill, M. Challacombe, P. M. W. Gill, B. Johnson, W. Chen, M. W. Wong, C. Gonzalez and J. A. Pople, *GAUSSIAN 03 (Revision C.02)*, Gaussian, Inc., Wallingford, CT, 2004.
31 P. Hamm, S. M. Ohline and W. Zinth, *J. Chem. Phys.*, 1997, **106**, 519–529.
32 J. Briand, *PhD thesis*, Strasbourg University, 2009.
33 A. Z. Szarka, N. Pugliano, D. K. Palit and R. M. Hochstrasser, *Chem. Phys. Lett.*, 1995, **240**, 25.
34 H. Chosrowjan, S. Taniguchi, N. Mataga, M. Unno, S. Yamauchi, N. Hamada, M. Kumauchi and F. Tokunaga, *J. Phys. Chem. B*, 2004, **108**, 2686.
35 B. Hou, N. Friedman, M. Ottolenghi, M. Sheves and S. Ruhman, *Chem. Phys. Lett.*, 2003, **381**, 549–555.
36 A. Kahan, O. Nahmias, N. Friedman, M. Sheves and S. Ruhman, *J. Am. Chem. Soc.*, 2007, **129**, 537–546.
37 G. Zgrablić, S. Haacke and M. Chergui, *Chem. Phys.*, 2007, **338**, 168.
38 S. L. Dexheimer, Q. Wang, L. A. Peteanu, W. T. Pollard, R. A. Mathies and C. V. Shank, *Chem. Phys. Lett.*, 1992, **188**, 61–66.
39 T. Kobayashi, T. Saito and H. Ohtani, *Nature*, 2001, **414**, 531–534.
40 Q. Wang, R. W. Schoenlein, L. A. Peteanu, R. A. Mathies and C. V. Shank, *Science*, 1994, **266**, 422–424.
41 L. Dhar, J. A. Rogers and K. A. Nelson, *Chem. Rev.*, 1994, **94**, 157.
42 W. T. Pollard, H. L. Fragnito, J. Y. Bigot, C. V. Shank and R. A. Mathies, *Chem. Phys. Lett.*, 1990, **168**, 239.
43 A. B. Myers, R. A. Harris and R. A. Mathies, *J. Chem. Phys.*, 1983, **79**, 603–613.
44 W. Fuss, S. A. Trushin and W. E. Schmid, *Res. Chem. Intermed.*, 2001, **27**, 447.
45 J. Réhault, V. Zanirato, J. Helbing and M. Olivucci, unpublished.
46 M. Vengris, M. A. van der Horst, G. Zgrabli, I. H. M. van Stokkum, S. Haacke, M. Chergui, K. J. Hellingwerf, R. van Grondelle and D. S. Larsen, *Biophys. J.*, 2004, **87**, 1848.
47 B. Dietzek, A. Yartsev and A. N. Tarnovsky, *J. Phys. Chem. B*, 2007, **111**, 4520–4526.
48 R. A. Mathies, C. H. Brito Cruz, W. T. Pollard and C. V. Shank, *Science*, 1988, **240**, 777–779.
49 L. A. Peteanu, R. W. Schoenlein, Q. Wang, R. A. Mathies and C. V. Shank, *Proc. Natl. Acad. Sci. U. S. A.*, 1993, **90**, 11762–11766.
50 R. W. Schoenlein, L. A. Peteanu, Q. Wang, R. A. Mathies and C. V. Shank, *J. Phys. Chem.*, 1993, **97**, 12087–12092.
51 G. Haran, E. A. Morlino, J. Matthes, R. H. Callender and R. M. Hochstrasser, *J. Phys. Chem. A*, 1999, **103**, 2202–2207.

52 Q. Wang, G. G. Kochendoerfer, R. W. Schoenlein, P. J. E. Verdegem, J. Lugtenburg, R. A. Mathies and C. V. Shank, *J. Phys. Chem.*, 1996, **100**, 17388–17394.
53 R. González-Luque, M. Garavelli, F. Bernardi, M. Merchán, M. A. Robb and M. Olivucci, *Proc. Natl. Acad. Sci. U. S. A.*, 2000, **97**, 9379–9384.
54 M. Ben-Nun, F. Molnar, K. Schulten and T. J. Martinez, *Proc. Natl. Acad. Sci. U. S. A.*, 2002, **99**, 1769–1773.
55 As a matter of fact, a third member of the NAIP family, the non-methoxylated NAIP, which presents unfortunately a significant E–Z mixture in the dark and at room temperature, has a sub-100 fs fluorescence lifetime and shows even more pronounced ground state oscillations (unpublished data).
56 V. I. Prokhorenko, A. M. Nagy, S. A. Waschuk, L. S. Brown, R. R. Birge and R. J. D. Miller, *Science*, 2006, **313**, 1257–1261.
57 G. Vogt, G. Krampert, P. Niklaus, P. Nuernberger and G. Gerber, *Phys. Rev. Lett.*, 2005, **94**, 068305.
58 B. J. Sussman, D. Townsend, M. Y. Ivanov and A. Stolow, *Science*, 2006, **314**, 278–281.
59 J. Bredenbeck, J. Helbing, C. Kolano and P. Hamm, *ChemPhysChem*, 2007, **8**, 1747–1756.